Polymer 99 (2016) 756–766

Contents lists available at ScienceDirect

Polymer

journal homepage: www.elsevier.com/locate/polymer

Correlation of intermolecular packing distance and crystallinity of D-A polymers according to π-spacer for polymer solar cells

Tae Ho Lee, Min Hee Choi, Sung Jae Jeon, Doo Kyung Moon*

Department of Materials Chemistry and Engineering, Konkuk University, 1 Hwayang-dong, Gwangjin-gu, Seoul 143-701, South Korea

ARTICLE INFO

Article history:
Received 17 May 2016
Received in revised form
23 July 2016
Accepted 28 July 2016
Available online 29 July 2016

Keywords:
Intermolecular distance
π-Spacer
Polymer shape

ABSTRACT

Donor–acceptor-type polymers, PBDPBT-T, PBDPBT-TT, and PBDPBT-biT, were polymerized via Stille coupling reactions. In the unfavorable mode of DFT calculations, the distance between BDP in the two different polymer main chains showed different distance of repeating unit (Dn) according to the π-spacers type. Especially, PBDPBT-TT caused larger D2 than PBDPBT-T and PBDPBT-biT. The UV–vis absorption spectra of PBDPBT-T and PBDPBT-biT films were red-shifted compared with the solution absorption, whereas that of a PBDPBT-TT film was blue-shifted. PBDPBT-T and PBDPBT-biT had high crystallinity and a tendency of face-on orientation. In contrast, PBDPBT-TT had low crystallinity. Owing to differences in packing formation, the polymers had different J_{SC} values. When a polymer solar cell device was fabricated through a solution process, PBDPBT-biT (in a 1:1.5 ratio with $PC_{70}BM$) exhibited a PCE of 4.50%, with a J_{SC} value of 8.6 mA/cm^2, a V_{OC} value of 0.88 V, and an FF value of 59.4%.

1. Introduction

Over the past few decades, organic semiconducting polymers have received considerable attention owing to their numerous advantages, such as easy structural transformations, light absorption and emission properties, low process price due to the availability of solution processes, and the potential for making light weight and flexible devices. Thus, organic semiconducting polymers have been applied to electronic and optoelectronic devices, such as light emitting diodes (LED) [1], thin film transistors (TFT) [2], solar cells [3,4], and optical sensors [5].

In general, the active layer of polymer solar cells (PSCs) has a bulk heterojunction (BHJ) configuration. To achieve high-efficiency in a BHJ solar cell, the main chain units and side chains of the alternating conjugated donor–acceptor (D-A) polymers should be tuned to obtain low-bandgap (LBG) donor polymers by push-pull effects [6,7]. The effects of chemical parameters increase carrier mobility, adjust energy levels, and change absorption region according to control bandgap. These studies have shown that high efficiency can be obtained by increasing the short-circuit current density (J_{SC}), open-circuit voltage (V_{OC}), and fill factor (FF) through changing the arrangement of polymers in the device. Recently, efficiencies are accomplished up to 10.6% in a single cell and maximum 11.7% in multi junction-cells [8,9]. And improved photon harvesting properties through device structure control have been reported [10]. The J_{SC} value of the PSCs with BHJ systems can be increased using the following method, which improves the electron mobility and compatibility with PCBM.

Adjusting the π-spacers in the conjugated π–bridge of D–A type LBG polymers for solar cells has recently drawn attention. The influence of increasing the conjugation length on the optical and electrical properties of D–A polymers has been widely studied. In particular, to achieve close packing of the polymers and thus good charge transport characteristics, the steric hindrance should be decreased for enhancing the planarity and intermolecular π–π interactions. Woo and Wang et al. reported change of the crystallites as introduced π-spacer such as thieno[3,2-*b*]thiophene (TT) and bithiophene (biT) [11,12]. Polymers with TT or biT spacers had increased crystallinity and higher J_{SC} owing to extended π-spacers and decreased steric hindrance. Moreover, extending the length of the π-spacer section enhanced the face-on orientation owing to decreased the steric hindrance, resulting in higher J_{SC}. In addition, the formation of face-on structures in polymer thin film was studied by controlling the stacking properties by changing the side chains, functional units, and π-spacers of the polymer. In PSCs, the face-on structure is more advantageous for transferring electric charge and increasing J_{SC} than the edge-on structure. Hou et al. reported that

* Corresponding author. Present address: Department of Materials Chemistry and Engineering, Konkuk University, 1 Hwayang-dong, Gwangjin-gu, Seoul 143-701, South Korea.
E-mail address: dkmoon@konkuk.ac.kr (D.K. Moon).

http://dx.doi.org/10.1016/j.polymer.2016.07.082
0032-3861/

the curvature of the polymer main backbone could be tuned with kind of polymer donor unit [13]. Polymers with a linear curvature polymers were shown to have a highly crystalline (010) peak and form the face-on orientation. In our previous work, we adjusted the length of the π-spacer (0–2) in polymers with alkylidenefluorene and isoindigo derivative to increase the J_{SC} through enhanced crystallinity [14]. We found a correlation between the structure of π-spacer and crystallinity, and by extension, polymer curvature.

Benzo[1,2-*b*;4,5-*b*′]dithiophene (BDT), which is a widely used, electron-rich donor unit, has the advantages of high hole mobility owing to its π-conjugated structure, planarity as a result of two thiophene (T) units fused with a benzene core, and solubility depending on the side chain [15,16]. Recent studies have reported PSCs with power conversion efficiencies (PCE) of 4–10% for BDT copolymerized with benzothiadiazole (BT), thieno[3,4-*b*]thiophene, diketopyrrolopyrrole (DPP), thiazolothiazole (TTZ), and thienopyrroledione (TPD) derivatives [17,18]. The benzo[2,1-*b*:3,4-*b*′]dithiophene (BDP) unit has similar characteristics to those of the BDT unit, but could allow different curvature of the molecular back bone to be achieved. In polymers, BDP has excellent electron mobility and may enable increased J_{SC} values by improving the blending properties and increasing the contact area with PCBM owing to zigzag or S-shape molecular arrangements [19–21].

Since the development of PSCs. BT has been used in D-A type polymers, such as PCDTBT and PFOBT, as an acceptor unit BT derivatives with octyloxy(BTO) have recently been used in many studies because of their enhanced solubility without considerable effects on the molecular arrangement or energy levels during device production [22].

In this study, D-A type polymers were synthesized using a BDP donor and BTO acceptor. T, TT and biT were introduced into the polymer main chain as π-spacers. The optical and electrochemical properties of the polymers were characterized and correlated to the curvature of the π-spacer. The results showed that the molecular curvature and arrangement of the polymer films were affected by the π-spacer. Additionally, the introduction of T and biT decreased steric hindrance in polymer backbone and increased electron mobility. By applying the polymer with biT spacer, as the active layer in a PSCs device, J_{SC} and FF were increased with optimized PCE of 4.50% and V_{OC} of around 0.88 V.

2. Experimental section

2.1. Measurements

Unless otherwise specified, all reactions were performed under a nitrogen atmosphere. The solvents were dried using the standard procedures. All column chromatography was performed with silica gel (230–400 mesh, Merck) as the stationary phase. ^{1}H NMR (400 MHz) spectra were recorded with a Bruker AMX400 spectrometer, using the resonances of the solvent as an internal reference. Chemical shifts (delta: d) are reported in ppm downfield from TMS. The molecular weights of the polymers were measured using the GPC method with polystyrene standards. TGA measurements were performed on a TA Instruments 2050 analyzer. Electrochemical cyclic voltammetry was performed using a Zahner IM 6e electrochemical workstation with 0.1 M Bu_4NPF_6 in acetonitrile as the electrolyte. ITO glass coated with a thin polymer film was used as the working electrode, and a Pt wire and an Ag/Ag^+ electrode were used as the counter and reference electrodes, respectively. The electrochemical potential was calibrated against Fc/Fc^+. Current–voltage (I–V) curves of the PSC devices were measured using a computer-controlled Keithley 2400 source measurement unit equipped with a Peccell solar simulator under AM1.5G illumination (100 mW/cm^2). The illumination intensity was calibrated using a standard Si photodiode detector equipped with a KG-5 filter. The output photocurrent was adjusted to match the photocurrent of the Si reference cell to obtain a power density of 100 mW/cm^2. After encapsulation, all devices were operated under ambient atmospheric conditions at 25 °C.

2.2. Fabrication and treatment of polymer solar cells

All of the BHJ PV cells were prepared using the following device fabrication procedure. The glass/indium tin oxide (ITO) substrates [Sanyo, Japan (10 X/c)] were lithographically patterned, cleaned with detergent, and sonicated in deionized water, acetone, and isopropyl alcohol. The substrates were then dried on a hot plate at 120 °C for 10 min and treated with oxygen plasma for 30 min to improve the contact angle immediately before the film coating process. Poly(3,4-ethylene-dioxythiophene): poly(styrene-sulfonate) (PEDOT:PSS, Baytron P 4083 Bayer AG) was passed through a 0.45-lm filter before being deposited onto the ITO substrates at a thickness of ca. 32 nm by spin-coating at 4000 rpm in air and then dried at 120 °C for 20 min inside a glove box. The solutions were then passed through a 0.45-lm PTFE filter and spin-coated (500–4000 rpm, 30 s) on top of the PEDOT:PSS layer device fabrication was completed by depositing layers of Al (200 nm) at pressures of less than 10^{-6} torr. The active area of the devices was 4.0 mm^2. Finally, the cell was encapsulated using a UV-curing glue (Nagase, Japan). The conventional devices were fabricated with the following structure: ITO glass/PEDOT:PSS/polymer:$PC_{70}BM$(active layer)/BaF_2/Ba/Al encapsulation glass. The inverted devices were fabricated with the following structure: ITO glass/ZnO/polymer:-$PC_{70}BM$(active layer)/MoO_3/Al encapsulation glass.

2.3. Synthesis

2.3.1. 4,5-Di(2-ethylhexyloxy)benzo[2,1-b:3,4-b′]dithiophene (**2**)

Compound 1 (0.35 g, 1.14 mmol), cesium carbonate (3.7 g, 11.42 mmol), and 2-ethylhexyl bromide (2.0 mL, 11.42 mmol) were dissolved in 20 mL acetonitrile. The reaction mixture was stirred at 75 °C. 2-ethylhexyl bromide and cesium carbonate were added more and the mixture was refluxed to 75 °C for further 24 h. The mixture was cooled to room temperature and acetonitrile was removed by rotary evaporation. The residue was partitioned between water and dichloromethane. The organic phase was washed with 1 M HCl and then with water, dried over Na_2SO_4. Evaporation of the solvent led to a brown oil. The product was purified by column chromatography (*n*-hexane–MC 1: 1). Pure product 2 (0.41 g, 0.912 mmol, 80%) was obtained as a white solid. ^{1}H NMR (400 MHz, $CDCl_3$): 7.50 (d, 2H), 7.35 (d, 2H), 4.06 (m, 4H), 1.81 (m, 2H), 1.67 (m, 2H), 1.55 (m, 6H), 1.36 (m, 8H), 0.95 (m, 13H). *m*/*z* 448.

2.3.2. 2,7-Bis(trimethyltin)-4,5-di(2-ethylhexyloxy)benzo[2,1-b:3,4-b′]dithiophene (**BDP**, **D1**)

Compound 2 (0.45 g, 1.0 mmol) was dissolved in 5 mL dry THF. The slightly yellow solution was cooled to −78 °C and *n*-BuLi (1.0 mL, 2.5 mmol, 2.5 M in *n*-hexane) was added over 30 min. The suspension was stirred for 1.0 h at −78 °C and 1.0 h at room temperature. After cooling to −78 °C trimethylstannyl chloride 1.0 M in THF (2.5 mL, 2.5 mmol) was added in one portion. The mixture was stirred for 1 h at −78 °C and at room temperature overnight. An ivory solution was formed and *n*-hexane were added for quenching. The suspension was washed with water, dried over Na_2SO_4 and the solvent was removed by evaporator. The product was dried in high vacuum to obtain 780 mg (0.68 mmol, 90%) of a white solid of D1, which was used in the next step without further purification. ^{1}H NMR (400 MHz, $CDCl_3$): 7.54 (s, 2H), 4.06 (d, 4H), 1.52 (t, 4H), 1.43 (s, 2H), 1.37 (m, 10H), 0.97 (t, 8H), 0.94 (m, 8H), 0.44 (t, 24H). *m*/*z* 772.

*2.3.3. 5,6-bis(octyloxy)-4,7-di(thiophen-2-yl)benzo[c][1,2,5] thiadiazole (**3**)*

A0 (0.826 g, 1.5 mmol), tributyl(thiophen-2-yl)stannane (1.231 g 3.3 mmol) and bis(triphenylphosphine)palladium(II) chloride (0.21 g, 0.3 mmol) were dissolved in 30 mL of anhydrous THF in a well-dried round flask under nitrogen atmosphere. After flushing with nitrogen, the reactant was heated to reflux for 24 h. After cooled to room temperature, the reaction mixture was poured into water. The product was extracted with ethyl acetate. The extracts were combined and washed with water and brine, then dried over Na_2SO_4. The filtrate was concentrated under reduced pressure. The residue was purified by column chromatography on silica to give compound as a deep red crystal (0.710 g, 85%). ^{1}H NMR (400 MHz, $CDCl_3$): δ (ppm) 8.47 (d, 2H), 7.50 (d, 2H), 7.23 (t, 2H), 4.10 (t, 4H), 1.91 (m, 4H), 1.41 (m, 4H), 1.34–1.29 (m, 16H), 0.89 (t, 6H). *m*/*z* 556.

*2.3.4. 5,6-bis(octyloxy)-4,7-di(thieno[3,2-b]thiophen-2-yl)benzo[c] [1,2,5]thiadiazole (**4**)*

A0 (0.826 g, 1.5 mmol), trimethyl(thieno[3,2-*b*]thiophen-2-yl) stannane (1.000 g 3.3 mmol) and bis(triphenylphosphine)palladium(II) chloride (0.21 g, 0.3 mmol) were dissolved in 60 mL of anhydrous THF in a well-dried round flask under nitrogen atmosphere. After flushing with nitrogen, the reactant was heated to reflux for 24 h. After cooled to room temperature, the reaction mixture was poured into water. The product was extracted with ethyl acetate. The extracts were combined and washed with water and brine, then dried over Na_2SO_4. The filtrate was concentrated under reduced pressure. The residue was purified by column chromatography on silica to give compound as a deep red oil(0.893 g, 89%). ^{1}H NMR (400 MHz, $CDCl_3$): δ (ppm) 8.80 (s, 2H), 7.46 (d, 2H), 7.31 (d, 2H), 4.16 (t, 4H), 1.98 (m, 4H), 1.455 (m, 4H), 1.33–1.28 (m, 16H), 0.89 (t, 6H). *m*/*z* 668.

*2.3.5. 4,7-di(2,2′-bithiophen-5-yl)-5,6-bis(octyloxy)benzo[c][1,2,5] thiadiazole (**5**)*

A0 (0.826 g, 1.5 mmol), 2,2′-bithiophen-5-yltrimethylstannane (1.086 g 3.3 mmol) and bis(triphenylphosphine)palladium(II) chloride (0.21 g, 0.3 mmol) were dissolved in 60 mL of anhydrous THF in a well-dried round flask under nitrogen atmosphere. After flushing with nitrogen, the reactant was heated to reflux for 24 h. After cooled to room temperature, the reaction mixture was poured into water. The product was extracted with ethyl acetate. The extracts were combined and washed with water and brine, then dried over Na_2SO_4. The filtrate was concentrated under reduced pressure. The residue was purified by column chromatography on silica to give compound as a deep red crystal(0.995 g, 92%). ^{1}H NMR (400 MHz, $CDCl_3$): δ (ppm) 8.51 (d, 2H), 7.31 (d, 2H), 7.29 (d, 2H), 7.27 (d, 2H), 7.07 (t, 2H), 4.17 (t, 4H), 1.98 (m, 4H), 1.50 (m, 4H), 1.36–1.29 (m, 16H), 0.88 (t, 6H). *m*/*z* 720.

*2.3.6. 4,7-bis(5-bromothiophen-2-yl)-5,6-bis(octyloxy)benzo[c] [1,2,5]thiadiazole (**A1**)*

Compound 3 (1.113 g, 2.0 mmol) was added to a mixture of chloroform (100 mL) and acetic acid (100 mL). After *N*-bromosuccimide (0.783 g, 4.4 mmol) was added, the mixture was stirred at room temperature in dark overnight. Then the reaction mixture was poured into water and extracted with chloroform. The extracts were combined and washed with water and saturate sodium bicarbonate solution then dried over Na_2SO_4. After filtration, the solvent in filtrate was removed under reduced pressure. The residue was purified by column chromatography on silica gel to give compound as a dark red crystal (1.26 g, 88%). ^{1}H NMR (CDCl3): δ (ppm) 8.37 (s, 2H), 7.18 (s, 2H), 4.12 (t, 4H), 1.94 (m, 4H), 1.45 (m, 4H), 1.36–1.30 (m, 16H), 0.90 (t, 6H). *m*/*z* 822.

*2.3.7. 4,7-bis(5-bromothieno[3,2-b]thiophen-2-yl)-5,6-bis(octyloxy)benzo[c][1,2,5]-thiadiazole (**A2**)*

Compound 4 (1.338 g, 2 mmol) was added to a mixture of chloroform (100 mL) and acetic acid (100 mL). After *N*-bromosuccimide (0.783 g, 4.4 mmol) was added, the mixture was stirred at room temperature in dark overnight. Then the reaction mixture was poured into water and extracted with chloroform. The extracts were combined and washed with water and saturate sodium bicarbonate solution then dried over Na_2SO_4. After filtration, the solvent in filtrate was removed under reduced pressure. The residue was purified by column chromatography on silica gel to give compound as a dark red oil (1.406 g, 85%). ^{1}H NMR (400 MHz, $CDCl_3$): δ (ppm) 8.75 (s, 2H), 7.33 (s, 2H), 4.15 (t, 4H), 1.96 (m, 4H), 1.45 (m, 4H), 1.33–1.25 (m, 16H), 0.89 (t, 6H). *m*/*z* 994.

*2.3.8. 4,7-bis(5′-bromo-2,2′-bithiophen-5-yl)-5,6-bis(octyloxy) benzo[c][1,2,5]-thiadiazole (**A3**)*

Compound 5 (1.442 g, 2 mmol) was added to a mixture of chloroform (100 mL) and acetic acid (100 mL). After *N*-bromosuccimide (0.783 g, 4.4 mmol) was added, the mixture was stirred at room temperature in dark overnight. Then the reaction mixture was poured into water and extracted with chloroform. The extracts were combined and washed with water and saturate sodium bicarbonate solution then dried over Na_2SO_4. After filtration, the solvent in filtrate was removed under reduced pressure. The residue was purified by column chromatography on silica gel to give compound as a dark red crystal (1.424 g, 81%). ^{1}H NMR ($CDCl_3$): δ (ppm) 8.50 (d, 2H), 7.23 (d, 2H), 7.03 (m, 4H), 4.16 (t, 4H), 1.96 (m, 4H), 1.49 (m, 4H), 1.33–1.29 (m, 16H), 0.89 (t, 6H). *m*/*z* 1046.

2.4. Polymerization

P-type monomer (BDP) (0.3 mmol), n-type monomer (A1-A3) (0.3 mmol), $Pd_2dba_3(0)$ (0.01 g, 0.012 mmol), and P(o-tolyl)$_3$ (0.0146 g, 0.048 mmol) were dissolved in toluene (10 mlL). The flask was degassed and refilled with nitrogen gas twice. The polymerization mixture was stirred at 90 °C for 48 h, and a small quantity 2-bromothiophene were added. After 6 h, a small quantity 2-tributylstannyl thiophene were also added for the end-capping reaction. The reaction mixture was cooled to room temperature and poured into methanol. The precipitate was filtered and purified with methanol, acetone, *n*-hexane and chloroform in a Soxhlet apparatus. The polymer was precipitated in methanol. Finally, the polymer was collected as a materials.

*2.4.1. Poly(4,5-di(2-ethylhexyloxy)benzo[2,1-b:3,4-b′]dithiophene-4,7-bis(thiophen-2-yl)-5,6-bis(octyloxy)benzo[c][1,2,5]thiadiazole) (**PBDPBT-T**)*

Dark red solid, yield = 78.2%. ^{1}H NMR (400 MHz, $CDCl_3$): δ (ppm) 7.75 (m), 7.45–7.23 (m), 7.10 (m), 4.07–3.90 (m), 2.17 (m), 2.10–0.89 (m).

*2.4.2. Poly(4,5-di(2-ethylhexyloxy)benzo[2,1-b:3,4-b′]dithiophene-4,7-bis(thieno[3,2-b]thiophen-2-yl)-5,6-bis(octyloxy)benzo[c][1,2,5] thiadiazole) (**PBDPBT-TT**)*

Dark brown solid, yield = 48.3%. ^{1}H NMR (400 MHz, $CDCl_3$): δ (ppm) 7.72 (m), 7.47–7.21 (m), 7.00 (m), 4.09–3.92 (m), 2.18 (m), 2.00–0.84 (m).

*2.4.3. Poly(4,5-di(2-ethylhexyloxy)benzo[2,1-b:3,4-b′]dithiophene-4,7-bis(2,2′-bithiophen-5-yl)-5,6-bis(octyloxy)benzo[c][1,2,5] thiadiazole) (**PBDPBT-biT**)*

Deep dark purple, yield = 76.5%. ^{1}H NMR (400 MHz, $CDCl_3$): δ (ppm) 8.25 (m), 7.36–7.23 (m), 6.96 (m), 4.25–3.87 (m), 2.17 (m), 2.00–0.84 (m).

3. Results and discussion

3.1. Synthesis and characterization of polymers

The chemical structures of synthetic routes to the monomers and polymers are described in Scheme 1. The monomers were synthesized according to literature methods [23,24]. 2,7-Bis(trimethyltin)-4,5-di(2-ethylhexyloxy)benzo[2,1-*b*:3,4-*b*′] dithiophene (**BDP**, **D1**) and 5,6-bis(octyloxy)benzo[c][1,2,5]thiadiazole (**A0**) were used as a donor and an acceptor, respectively. In addition, T, TT, and biT were introduced as π-spacer for A0 to synthesize 4,7-bis(5-bromothiophen-2-yl)-5,6-bis(tetradecyloxy) benzo[c][1,2,5]thiadiazole (**BT-T, A1**), 4,7-bis(5-bromo-thieno[3,2-*b*]thiophen-2-yl)-5,6-bis(octyloxy) benzo[c][1,2,5]thiadiazole (**BT-TT, A2**), and 4,7-bis-(5-bromo-[2,2′]bithiophenyl-5-yl)-5,6-bis-octyloxy- benzo[c][1,2,5]thiadiazole (**BT-biT, A3**), respectively, as shown in Scheme 1. Poly(4,5-di(2-ethylhexyloxy)benzo[2,1-*b*:3,4-*b*′]dithiophene-alt-spacer-5,6-bis(octyloxy)benzo[c][1,2,5] thiadiazole (**PBDPTB-T, PBDPTB-TT, and PBDPTB-biT**) were polymerized via the Stille coupling reaction of **D1** and the benzo[c] [1,2,5]thiadiazole derivatives (**A1**–**A3**) [25]. The obtained polymers were dark red, dark brown, and deep dark purple powders with yields of 78.2%, 48.3%, and 76.5% for polymers (-T, -TT, -biT), respectively. PBDPBT-T and PBDPBT-biT were soluble in general organic solvents, such as chloroform, chlorobenzene, and *o*-dichlorobenzene (ODCB). However, PBDPBT-TT had a relatively low molecular weight and low solubility. PBDPBT-TT dissolved only in chloroform and ODCB at elevated temperature. This result is similar tendency to the trends observed for various results of π-spacers by Li and Zhang [26,27]. The synthesized monomer and polymer structures were identified using ^{1}H NMR and GC-MS (Experimental section).

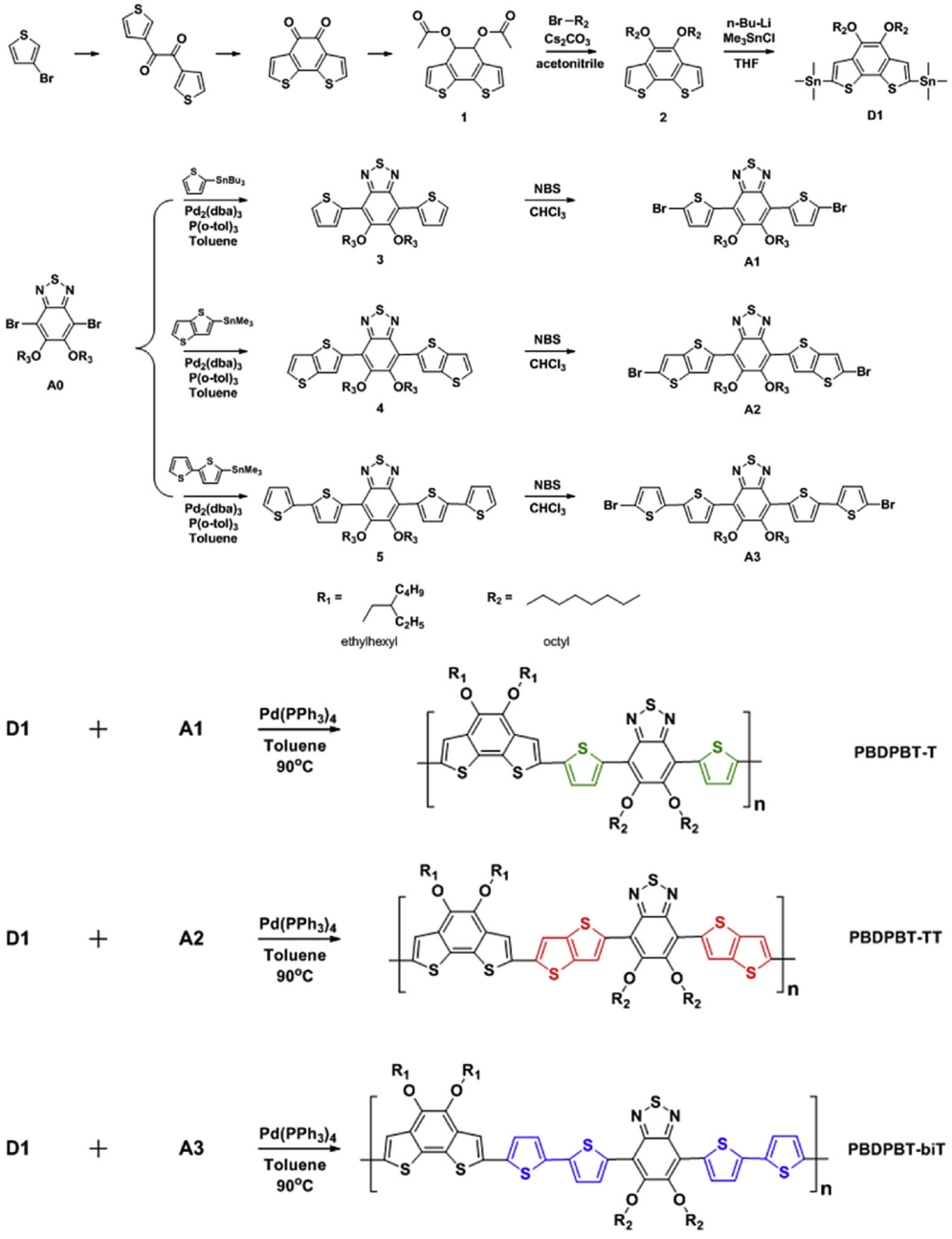

Scheme 1. Synthesis and characterization of monomers and polymers.

Table 1
Physical and thermal properties of polymers.

Polymer	Mn[a] [kDa]	Mw[a] [kDa]	PDI[a]	Degree of polymerization	T_d(°C)
PBDPBT-T	23.6	28.1	1.51	23.6	309
PBDPBT-TT	9.6	27.9	2.91	7.8	302
PBDPBT-biT	21.3	34.8	1.63	18.3	305

[a] Determined by GPC in Chloroform using polystyrene standards.

3.2. Molecular and thermal properties

The measured molecular weights of the polymers are shown in Table 1. The number average molecular weights (Mn) values for polymers (-T, -TT, -biT) were 23,600, 9,600, and 21,300 g/mol, respectively, with corresponding PDI values of 1.51, 2.91, and 1.63. In a previous study, our group reported relationship between spacer and solubility in D-A type polymers. However, in this study, TT gave different results. PBDPBT-TT was observed to have a relatively low molecular weight and solubility because of precipitation during the polymerization process, which is similar to the findings of Andersson [28]. As shown in Table 1 and Fig. S9, the transition temperatures (T_d) of polymers (-T, -TT, -biT) in a N_2 atmosphere were quite similar at 309, 302, and 305 °C, respectively. All of the polymers exhibited excellence thermal stability, indicating their suitability for optoelectronic device fabrication and application.

3.3. Photophysical properties

UV–vis spectra of the chloroform solution and spin-coated thin films are shown in Fig. 1 and summarized in Table 2. The molar absorption coefficients (ε) were calculated by measuring the UV–vis absorbance in solution (Fig. S10). Each polymer displayed two absorption peaks. The low energy band absorption peak (λ_{max} = 500–600 nm) is caused by intramolecular charge transfer (ICT) between the donor and acceptor units, whereas the high energy band absorption peak (λ_{max} = 300–400 nm) is caused by localized π–π^* transitions [29].

Although these three polymers contain the same D–A units, different absorption intensities were obtained, depending on the π–spacer. As shown in Fig. 1a, the π–π^* transition peaks of the polymers in solution increased and ICT absorption peaks decreased in the order biT, T and TT. This result indicated that TT spacer disrupted charge transfer in the polymer chain, resulting in a low ICT effect in PBDPBT-TT. The ε value of PBDPBT-biT was the highest (49,400 M^{-1} cm^{-1}), indicating that it facilitates greater optical absorption. Moreover, the absorption coefficients of PBDPBT-T (42,500 M^{-1} cm^{-1}) and PBDPBT-biT were approximately 1.5 times larger than that of PBDPBT-TT (30,300 M^{-1} cm^{-1}), which is a result of the planarity of the polymers. Polymers with planar structures and high molecular weights have strong intermolecular π–π stacking interactions. Thus, charge transfer and π–π^* electron transitions are favorable and exceptionally high molar absorptivity can be achieved. This result is consistent with the findings of Icil and Hoffmann [30,31].

Fig. 1b shows the UV–vis spectra of the polymers in the film state. In the film phase, the absorption peaks of PBDPBT-T and PBDPBT-biT were red-shifted by 16 and 11 nm compared to the solution phase, respectively. In addition, a shoulder can be observed between 600 and 650 nm, which is the result of narrow intermolecular distances due to the planarity of the polymer main chain. The intermolecular distance decreases in the film state compared with than in the solution state because of aggregation in the solid state. In contract, the absorption peak of PBDPBT-TT in the film state was blue-shifted by 7 nm. This is a result of steric hindrance between the polymer chains, which disturbs the intermolecular overlap of π-electrons. Similar results were obtained in previous studies by our group [14,32] and others, including Matzger, Watson, and Corminboeuf [33–35]. Compared with the TT spacer, the T and

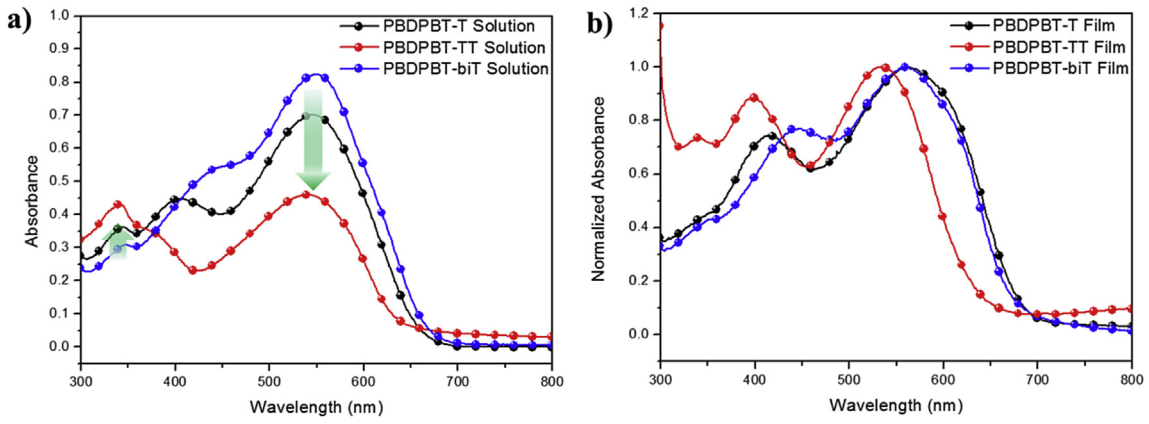

Fig. 1. UV–vis absorption of the polymers a) in chloroform solution and b) thin film.

Table 2
Optical and electrochemical properties of the polymers.

Polymer	UV–vis absorption				$E_g^{op,a}$ [eV]	Cyclic voltammetry	
	$CHCl_3$ solution		Film			HOMO[b] [eV]	LUMO[a] [eV]
	λ_{max} [nm]	ε at λ_{max}	λ_{max} [nm]	λ_{onset} [nm]			
PBDPBT-T	546	42,500	418, 562	678	1.83	−5.31	−3.48
PBDPBT-TT	341, 541	49,400	398, 534	628	1.97	−5.29	−3.32
PBDPBT-biT	550	30,300	448, 561	672	1.85	−5.35	−3.50

[a] Calculated from the intersection of the tangent on the low energetic edge of the absorption spectrum with the baseline.
[b] $E_{HOMO\ (or\ LUMO)} = -[E_{onset}(vs\ Ag/AgCl) - E_{1/2}(Fc/Fc^+\ vs\ Ag/AgCl)] - 4.8e\ V$.

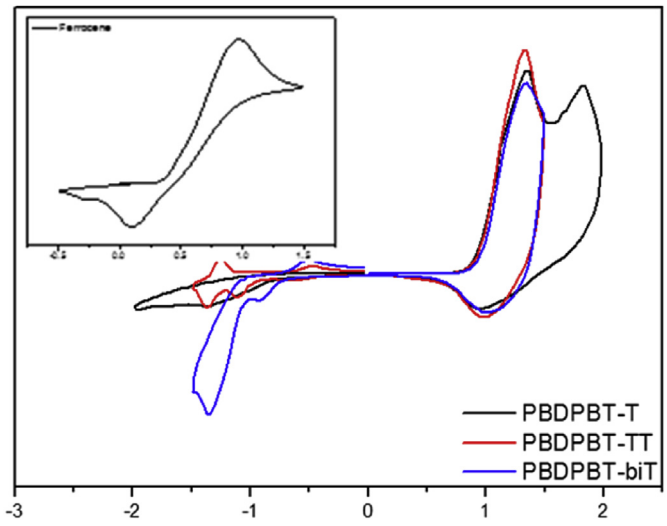

Fig. 2. Cyclic voltammograms of polymers and reference (Fc/Fc^{+}).

biT spacers cause more planar organization between the donor and acceptor units in the main chains of the polymer, and thus the T and biT spacers induces orderly π-π stacking. These results are consistent with the X-ray diffraction patterns in Section 3.4.

The cyclic voltammetry (CV) results are shown in Fig. 2 and summarized in Table 2. The oxidation onset potentials (E^{ox}_{onset}) of polymers (-T, -TT, -biT) were +0.92, +0.90, and +0.96 V, respectively, and the HOMO energy levels were measured to be −5.31, −5.29, and −5.35 eV, respectively. These results verified that the identity of the π-spacer does not greatly affect the HOMO (⊿0.06 eV) because the D-A derivatives in the main chain are fixed. These results are consistent with the work of Zhu et al. Using the same materials, the little difference in the HOMO was observed (⊿0.07 eV) as the number of π-spacers increased from one to three [13]. Because the air oxidation threshold is −5.27 eV, the HOMO of a material should be less than this value to have oxidation stability. Thus, these polymers are expected to have excellent oxidation stability. The LUMO is calculated from the UV band gap. The obtained bandgap trend is in agreement with the research of Brocks et al., who reported that with increasing π-conjugation length, the

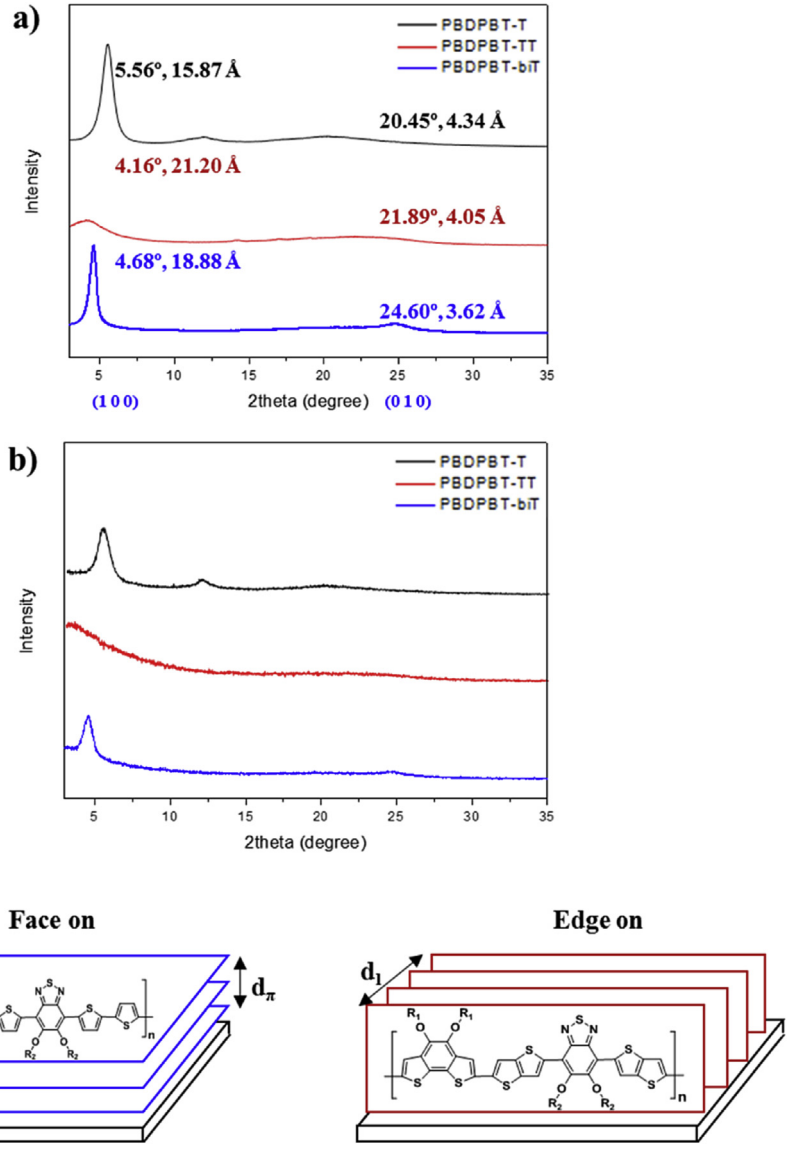

Fig. 3. X-ray diffraction patterns of the polymer films on a) out-of-plane mode and b) in-plane.

band gap was reduced according to the degree of polymerization [36].

3.4. X-ray analysis

The XRD spectra of the polymer films measured using the out-of-plane mode are shown in Fig. 3a. The (100) diffraction peak of the PBDPBT-T and PBDPBT-biT thin films occurred at 5.56° and 4.68°, respectively. The d-spacing (d_1) calculated using Bragg's law ($\lambda = 2d\sin\theta$) were 15.87 and 18.88 Å, respectively, which is consistent with the formation of highly ordered (100) lamellar structures. However, PBDPBT-TT showed a relatively low diffraction peak for the (100) plane at 4.16°, with a correspondingly high d_1 value of 21.2 Å. Diffraction peaks of the (010) crystal plane related to π–π stacking of polymers(-T, -TT, -biT) were observed at 20.45°, 21.89°, and 24.60°, respectively. The calculated π–π stacking distances (d_π) were 4.34, 4.05, and 3.62 Å, respectively. Thus, more effective intermolecular π-electron overlap can occur in PBDPBT-biT when compared with the other two polymers [37,38]. These results indicate that the polymers can form both (h00) and (0h0) lamellar structures.

The XRD spectra of the polymer thin films obtained using the in-plane mode are shown in Fig. 3b. For PBDPBT-TT, no diffraction peaks were observed. However, PBDPBT-T and PBDPBT-biT showed a strong crystal peak at a low angle. Based on the XRD peaks mentioned above, PBDPBT-T and PBDPBT-biT have face-on orientation and strong crystallinity, whereas PBDPBT-TT has a weak edge-on orientation and low crystallinity.

These results were consistent with the observation of a shoulder in the UV–vis spectra of PBDPBT-T and PBDPBT-biT thin films owing to interactions between molecules, whereas PBDPBT-TT does not show a shoulder peak in either solution or film. This difference is due to the influence of the spacer, which results in linear polymer backbones for PBDPBT-T and PBDPBT-biT, whereas that of PBDPBT-TT is curved. Moreover, it was confirmed that effective π–π stacking occurs for PBDPBT-T and PBDPBT-biT, as steric hindrance is reduced at lower dihedral angles. These results can be further verified by DFT calculations (Section 3.5). The π–π stacking of the face-on crystalline pattern and the planar backbone structure facilitate intermolecular electron transfer between polymer chains. Thus, materials with such structures are expected to show high J_{SC} values [39–41].

3.5. Electronic structure calculations

Simulations were carried out to determine the electrical properties, molecular geometries, and HOMO and LUMO electron distributions of the synthetic polymers. Density functional theory (DFT) calculations were performed using Gaussian 09 with the Hybrid B3LYP correlation functional and split valence 6-31G (d) basis set. Oligomers with repeat units of alkyl chains substituted by methyl groups were selected for ease of calculation. The calculated HOMO and LUMO orbitals and the geometries are presented in Figs. 4 and S11 and summarized in Table 3.

As shown in Fig. S3, the electronic cloud of the HOMO is delocalized over the entire polymer main backbone. However, the electronic cloud of the LUMO is localized on the acceptor monomer containing BT and the spacer. This is because of an accepting effect caused by the quinoid structure that forms between the conjugated electron pair on N and the electron-withdrawing S [12,42]. The results of the DFT calculations showed that all the polymers had a tendency for push-pull electron transfer in the main chain. The

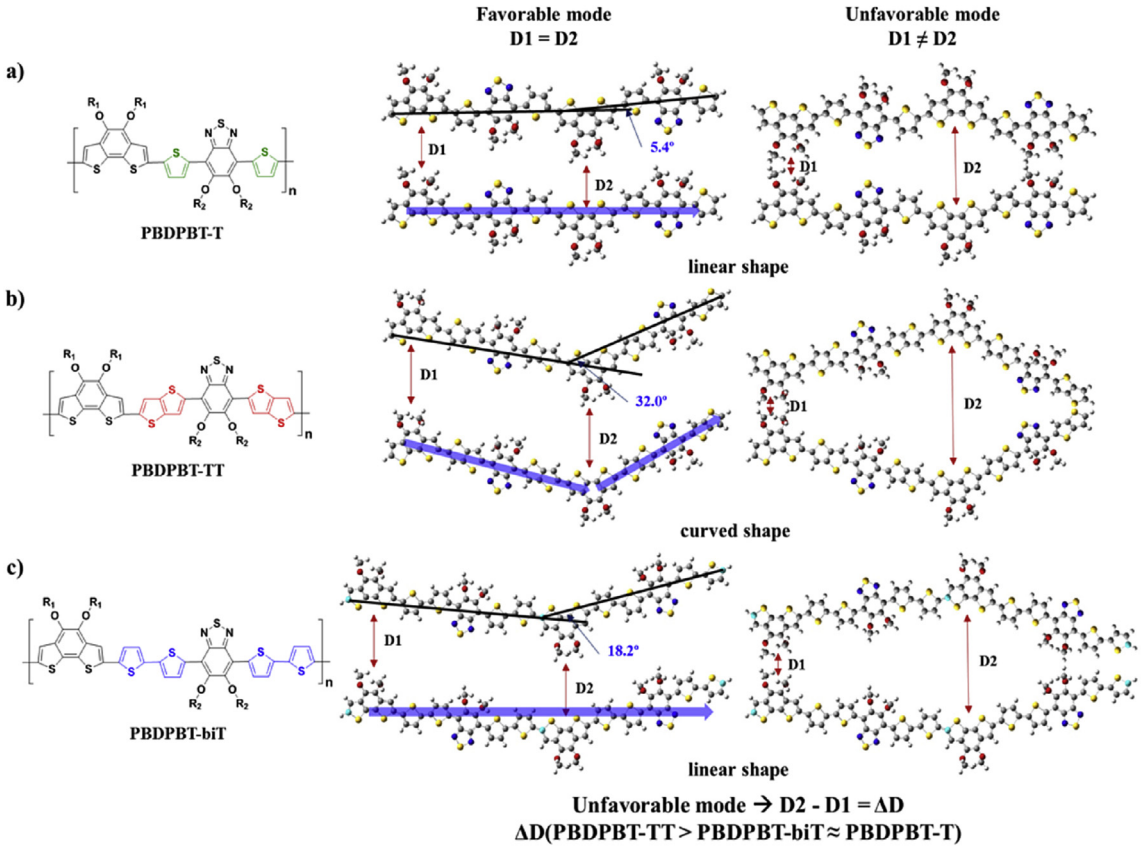

Fig. 4. The demonstration of the top views of the polymer packing modes from DFT calculate a) PBDPBT-T, b) PBDPBT-TT, and c) PBDPBT-biT.

Table 3
Calculated DFT parameters.

Polymer	Dihedral angle (deg)					Curved angle (deg)	HOMO$^{cal.}$ [eV]	LUMO$^{cal.}$ [eV]
	θ_1	θ_2	θ_3	θ_4	θ_5			
PBDPBT-T	8.42	14.09	8.89	–	–	5.4	−4.99	−2.55
PBDPBT-TT	12.86	13.95	8.25	–	–	18.2	−4.95	−2.64
PBDPBT-biT	8.22	14.06	5.72	4.58	8.35	32.0	−4.83	−2.63

HOMO and LUMO of polymers (-T, -TT, -biT) were calculated to be −4.99/−2.55, −4.98/-2.64, and −4.83/-2.63 eV, respectively. The HOMO energy levels of the three polymers are similar, which is consistent with the CV results, because the main donor and acceptor units are same in each polymer. As the conjugation length of the main chain increased in the order T, TT, and biT, the bandgap value decreased. As the number of oligomers increased, the bandgap also decreased owing to extension of the conjugation [43,44]. However, these calculation results do not match the bandgaps calculated as E_{onset} in the UV−vis spectra. This is due to the different polymerization degrees of the synthetic polymers. The polymerization degrees of polymers (-T, -TT, -biT) were 23.6, 7.5, and 18.3, respectively. In the case of PBDPBT-TT, the optical bandgap (E_g^{opt} = 1.97 eV) was measured relatively higher than its own E_g^{opt} because of its low polymerization degree. The dihedral angle of each polymer was around 4.58−14.09° and the conformation was locked due to interactions among the S of the thiophene spacer, N and O of BT, and S and O of BDP. This result verified that the overall shape of the polymer repeating unit was planer.

However, when two repeating units are examined, as shown in Fig. 5, the structural arrangement calculation results showed different characteristics for the packing mode of the polymers. In the favorable mode, PBDPBT-T and PBDPBT-biT formed linear backbone conformations, whereas PBDPBT-TT formed a curved backbone conformation. The angles of curvature of 5.4° and 18.2°in PBDPBT-T and PBDPBT-biT, respectively, showed that these polymers have planar structure that can form ordered inter-chain packing. This is consistent with the XRD results that showed good crystallinity with a strong (100) peak and face-on orientation. On the other hand, since the angle of curvature in PBDPBT-TT is much larger at 32.0°, it is difficult to obtain an evenly arranged thin film on the substrate and thus, this material showed low crystallinity. In the unfavorable mode, the distance (Dn, n = number of repeating units, 1 and 2) between BDP and BDP in the two main chains were changed (D1≠D2). In particular, PBDPBT-TT showed larger D2 and ⊿D (D2−D1) values than the other two polymers. The larger ⊿D value for PBDPBT-TT was bigger than that of PBDPBT-T and PBDPBT-biT. It was difficult to achieve face-to-face π−π stacking between molecules. Thus, the PBDPBT-TT film had a weak peak in XRD. In addition, such curved molecular structure has the disadvantage of forming a nanophase morphology in BHJ active layers [45,46]. In other words, such molecular structures causes weak interaction, which is consistent with a reduced intermolecular transfer.

3.6. Photovoltaic properties

J−V curves and incident photon to current efficiency (IPCE) spectra of the polymer photovoltaic devices are presented in Fig. 5

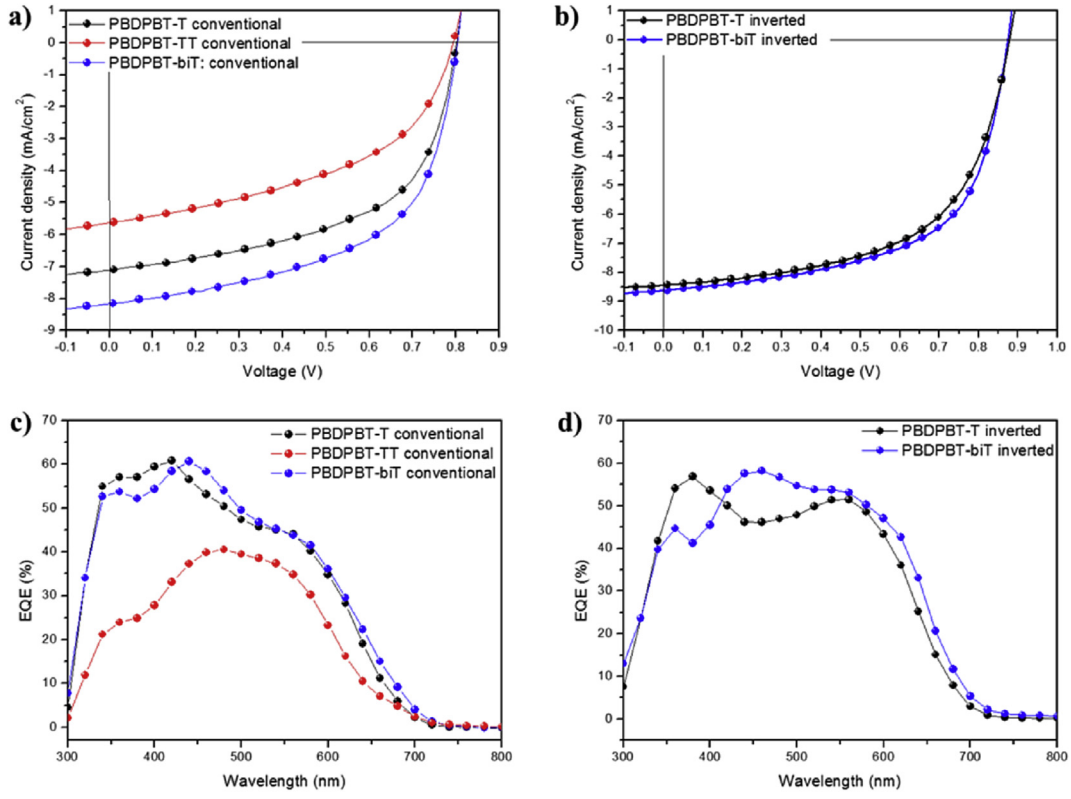

Fig. 5. J−V characteristics at a) conventional and b) inverted and external quantum efficiency at c) conventional and d) inverted of photovoltaic devices.

Table 4
Photovoltaic properties of polymers.

Polymer		$PC_{70}BM$ ratios	J_{SC} (mA/cm^2)	V_{OC} (V)	FF (%)	PCE (%)	J_{SC} at IPCE (mA/cm^2)
PBDPBT-T	Conventional	1:2	7.1	0.80	56.2	3.19	7.01
	Inverted	1:1.5	8.5	0.88	57.7	4.32	8.03
PBDPBT-TT	Conventional	1:2	5.6	0.80	47.6	2.13	5.33
PBDPBT-biT	Conventional	1:2	8.3	0.80	51.7	3.43	7.81
	Inverted	1:1.5	8.6	0.88	59.4	4.50	8.39

and the results are summarized in Table 4. The PCEs of polymers (-T, -TT, -biT) were 3.19, 2.13 and 3.43%, respectively in conventional device. The PCEs of polymers (-T, biT) were 4.32, and 4.50%, respectively, in inverted devices. These polymers had similar V_{OC} values in both types of devices (conventional - 0.80 V inverted −0.88 V). The V_{OC} of the fabricated devices showed a similar trend to that for the HOMO level measured by CV and DFT. The work function of the interlayer plays an important role because of the potential-energy alignment of the active layer and metal electrode. Compared with BaF_2 in a conventional device, electron transport layer (ZnO) in an inverted device increases the built in potential energy. Such a difference results in increases of V_{OC} [47,48]. The surface potential difference (ΔSP) of the active layer vs BaF_2 and ZnO films was measured using EFM to identify the energy level matching between the active layer and electron transport layer, as shown in Fig. S12. At the interface between the two layers in conventional and inverted devices, ΔSP of the two distinct parts changed. The ΔSP of PBDPBT-T:PCBM vs. BaF_2 and ZnO were 18.912 and 8.240 mV, respectively, whereas those of PBDPBT-biT:PCBM vs. BaF_2 and ZnO were 19.525 and 4.559 mV, respectively. At the interface of the two layers, ΔSP of the two distinct parts changed by 10.668 and 14.966 mV. This signifies that a smaller potential difference between the active layer and interlayers increased the probability of dissociation of excitons, leading to the improved V_{OC}. As PBDPBT-T and PBDPBT-biT have linear and planar structures, they are enhanced in structures with face-on orientation. Because of this, the J_{SC} values of these polymers were improved by 26.8% and 48.2%, respectively, compared with that of PBDPBT-TT.

The external quantum efficiency (EQE) was measured for the J_{SC} measurements, and these devices showed a sufficiently broad EQE graph in the visible range (300–700 nm) as shown in Fig. 6c and d. The EQE value was high in the range of 300–700 nm, but begins to decrease over 600 nm. PBDPBT-T and PBDPBT-biT had EQE_{max} values of 60.8% and 60.7%, respectively, but PBDPBT-TT had a lower EQE_{max} value of 40.5%. This is because of the increase of exciton recombination caused by poorer blending with PCBM due to low π–π stacking property and the curved shape of PBDPBT-TT [49,50]. When we manufactured inverted PSCs devices, PBDPBT-T and PBDPBT-biT showed slightly increased J_{SC} values. As shown in the EQE spectra of the inverted PSCs in Fig. 5d, a high EQE value is obtained for photon-electron conversion over 500 nm. The J_{SC} value can be calculated using the integral value of the EQE graph. The calculated J_{SC} values were explained Table 4 which is similar to the values measured from the J–V curve.

3.7. Hole mobility and morphological properties

In BHJ solar cells, J_{SC} and FF are directly limited by the hole mobility of the polymer. We determined the hole mobility using the space charge limited current (SCLC) method, as shown in Fig. S13 and summarized in Table S1. The hole mobility values of the polymers (-T, -TT, -biT) blended with $PC_{70}BM$ were 1.64×10^{-4}, 7.61×10^{-5}, and 2.74×10^{-4} cm^2/Vs, respectively. The hole mobility of the polymers was greatly affected by the crystal structure of the polymer film, which influences the charge-transfer pathway.

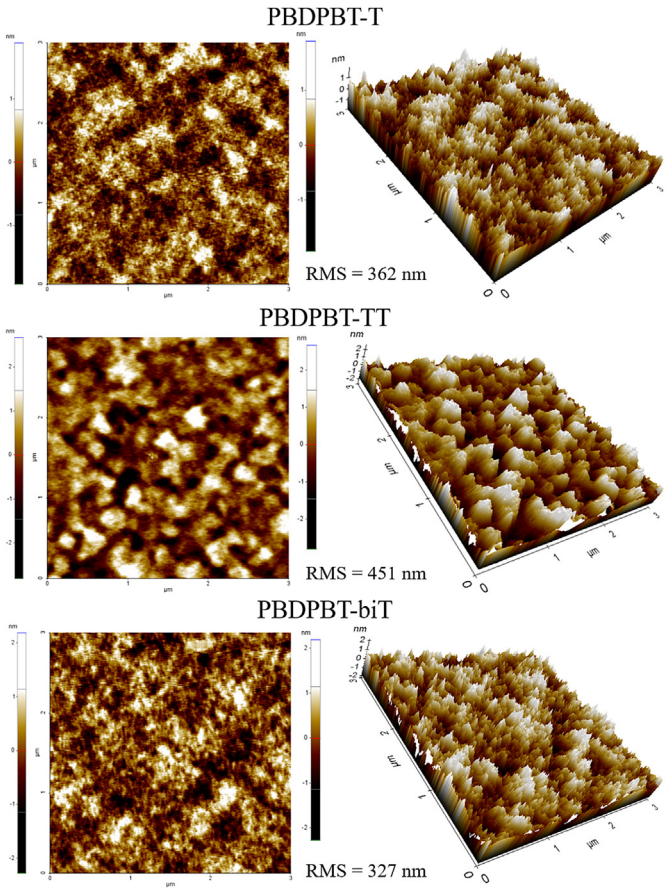

Fig. 6. Topographic AFM images of polymer:$PC_{70}BM$(1:2 w/w%) blend films.

PBDPBT-T and PBDPBT-biT, which were shown in XRD and DFT measurements to have face-on orientation, had higher hole mobilities, which led to high J_{SC} in the fabricated photovoltaic cell.

The surface morphology of a polymer blend is a critical factor in determining the efficiency of PSCs. Thus, atomic force microscopy (AFM) measurements of the polymer:$PC_{70}BM$ (1:2 w/w) blend films were obtained, as shown in Fig. 6. The dark colored and light-colored areas correspond to $PC_{70}BM$ domains and polymers, respectively. The PBDPBT-biT:$PC_{70}BM$ blend film showed a domain size of 20–40 nm with a small root-mean-square (RMS) roughness of 0.327 nm. The good intermixing between the polymer and $PC_{70}BM$ promoted the formation of nano-network channels and a smooth morphology. In contrast, the PBDPBT-T:$PC_{70}BM$ blend film had a domain size of 50–70 nm with a RMS roughness of 0.362 nm and the PBDPBT-TT:$PC_{70}BM$ blend film had a domain size of 100–150 nm with a RMS roughness of 0.451 nm. Rougher morphologies show low photocurrents owing to reduced charge separation in the active layer and an increasing exciton diffusion length for recombination [51,52]. The rougher morphology with PBDPBT-TT is a result of steric hindrance arising from the curved

structure, which is consistent with the lower photocurrent observed for PBDPBT-TT in comparison with PBDPBT-T and PBDPBT-biT. In addition, the result is consistent with the steric hindrance and shape curvature calculated by DFT.

4. Conclusion

In this study, we polymerized D-A-type polymers, such as PBDPBT-T, PBDPBT-TT, and PBDPBT-biT using Stille cross coupling. In each polymer, the individual repeating units showed an overall planar structure in DFT calculations. However, when oligomers with two repeating units were calculated, PBDPBT-TT had a curved shape and arrangement of molecules in a film became difficult. In the unfavorable mode, the distance (Dn, n = 1 and 2) between BDP in the two main chains, and ΔD values increased compared with those of the other two polymers. This result verified the blue shift of the UV–vis absorption in the film compared with that in solution. The polymers with T and biT as π-spacers formed planar and linear conformations and showed face-on orientation resulting in highly crystalline structures in the pristine polymer films. Thus, the π-spacer not only increases the π-conjugation length of the D-A monomer, but also determines the shape of the polymer main backbone. The polymer shape plays an important role in intermolecular π-electron overlap and greatly affects the crystallinity of the polymer film.

Acknowledgments

This paper was written as part of Konkuk University's research support program in 2014.

Appendix A. Supplementary data

Supplementary data related to this article can be found at http://dx.doi.org/10.1016/j.polymer.2016.07.082.

References

[1] M.A. Mohd Sarjidan, H.A. Mohd Mokhtar, W.H. Abd Majid, Determination of energy band diagram and charge carrier mobility of white emitting polymer from optical, electrical and impedance spectroscopy, J. Luminescence 159 (2015) 134–138.
[2] B. Nketia-Yawson, H.-S. Lee, H.J. Son, B. Kim, Y.-Y. Noh, Bar-coated high-performance organic thin-film transistors based on ultrathin PDFDT polymer with molecular weight independence, Org. Electron. 29 (2016) 88–93.
[3] E. Zhou, M. Nakano, S. Izawa, J. Cong, I. Osaka, K. Takimiya, K. Tajima, All-polymer solar cell with high near-infrared response based on a naphthodithiophene diimide (NDTI) copolymer, ACS Macro Lett. 29 (9) (2014) 872–875.
[4] Y. Li, Molecular design of photovoltaic materials for polymer solar cells: toward suitable electronic energy levels and broad absorption, Acc. Chem. Res. 29 (5) (2012) 723–733.
[5] V. Torres-Zúñiga, O.G. Morales-Saavedra, A.L. Pérez-Martínez, Fabrication and optical testing of hybrid SiO2: azo-polymer based planar waveguides for NLO/SHG laser emission, J. Phys. Conf. Ser. 582 (2015) 012001.
[6] P. Homyak, Y. Liu, F. Liu, T.P. Russel, E.B. Coughlin, Systematic variation of fluorinated diketopyrrolopyrrole low bandgap conjugated polymers: synthesis by direct arylation polymerization and characterization and performance in organic photovoltaics and organic field-effect transistors, Macromolecules 48 (19) (2015) 6978–6986.
[7] Y. Li, B. Xu, H. Li, W. Cheng, L. Xue, F. Chen, H. Lu, W. Tian, Molecular engineering of copolymers with donor–acceptor structure for bulk heterojunction photovoltaic cells toward high photovoltaic performance, J. Phys. Chem. C 115 (5) (2011) 2386–2397.
[8] C.C. Chen, W.H. Chang, K. Yoshimura, K. Ohya, J. You, J. Gao, Z. Hong, Y. Yang, An efficient triple-junction polymer solar cell having a power conversion efficiency exceeding 11%, Adv. Mater. 26 (32) (2014) 5670–5677.
[9] J. You, L. Dou, K. Yoshimura, T. Kato, K. Ohya, T. Moriarty, K. Emery, C.C. Chen, J. Gao, G. Li, Y. Yang, A polymer tandem solar cell with 10.6% power conversion efficiency, Nat. Commun. 4 (2013) 1446.
[10] K.G. Lim, M.R. Choi, J.H. Kim, D.H. Kim, G.H. Jung, Y. Park, J.L. Lee, T.W. Lee, Role of ultrathin metal fluoride layer in organic photovoltaic cells: mechanism of efficiency and lifetime enhancement, ChemSusChem 7 (4) (2014) 1125–1132.
[11] W. Lee, G.-H. Kim, S.-J. Ko, S. Yum, S. Hwang, S. Cho, Y.-H. Shin, J.Y. Kim, H.Y. Woo, Semicrystalline d–a copolymers with different chain curvature for applications in polymer optoelectronic devices, Macromolecules 47 (5) (2014) 1604–1612.
[12] X. Wang, Y. Sun, S. Chen, X. Guo, M. Zhang, X. Li, Y. Li, H. Wang, Effects of π-conjugated bridges on photovoltaic properties of donor-π-acceptor conjugated copolymers, Macromolecules 45 (3) (2012) 1208–1216.
[13] Q. Tao, Y. Xia, X. Xu, S. Hedström, O. Bäcke, D.I. James, P. Persson, E. Olsson, O. Inganäs, L. Hou, W. Zhu, E. Wang, D–A1–D–A2Copolymers with extended donor segments for efficient polymer solar cells, Macromolecules 48 (4) (2015) 1009–1016.
[14] M.-H. Choi, K.W. Song, D.K. Moon, Alkylidenefluorene–isoindigo copolymers with an optimized molecular conformation for spacer manipulation, π–π stacking and their application in efficient photovoltaic devices, Polym. Chem. 6 (14) (2015) 2636–2646.
[15] Y. Koizumi, M. Ide, A. Saeki, C. Vijayakumar, B. Balan, M. Kawamoto, S. Seki, Thienoisoindigo-based low-band gap polymers for organic electronic devices, Polym. Chem. 4 (3) (2013) 484–494.
[16] W. Li, K.H. Hendriks, A. Furlan, M.M. Wienk, R.A. Janssen, High quantum efficiencies in polymer solar cells at energy losses below 0.6 eV, J. Am. Chem. Soc. 137 (6) (2015) 2231–2234.
[17] F. Livi, N.K. Zawacka, D. Angmo, M. Jørgensen, F.C. Krebs, E. Bundgaard, Influence of side chain position on the electrical properties of organic solar cells based on dithienylbenzothiadiazole-alt-phenylene conjugated polymers, Macromolecules 48 (11) (2015) 3481–3492.
[18] Y.-L. Yang, Y.-H. Lee, Y.-P. Lee, C.-J. Chiang, F.-Y. Hsu, W.-C. Hsu, M.-k. Leung, L. Wang, C.-A. Dai, Y. Ohta, T. Yokozawa, Band gap tuning of narrow-polydispersity two-dimensional conductive polymers with electroactive side-chains, J. Polym. Sci. Part A Polym. Chem. 52 (9) (2014) 1217–1227.
[19] Y.Y. Liang, Y. Wu, D.Q. Feng, S.T. Tsai, H.J. Son, G. Li, L.P. Yu, Development of new semiconducting polymers for high performance solar cells, J. Am. Chem. Soc. 131 (1) (2009) 56–57.
[20] W. Yue, R.S. Ashraf, C.B. Nielsen, E. Collado-Fregoso, M.R. Niazi, S.A. Yousaf, M. Kirkus, H.Y. Chen, A. Amassian, J.R. Durrant, I. McCulloch, A thieno[3,2-b][1]benzothiophene isoindigo building block for additive- and annealing-free high-performance polymer solar cells, Adv. Mater. 27 (32) (2015) 4702–4707.
[21] Z.-G. Zhang, Y. Li, Side-chain engineering of high-efficiency conjugated polymer photovoltaic materials, Sci. China Chem. 58 (2) (2014) 192–209.
[22] F.A. Arroyave, C.A. Richard, J.R. Reynolds, Efficient Synthesis of benzo[1,2-b:6,5-b′]dithiophene-4,5-dione (BDTD) and its chemical transformations into precursors for pi-conjugated materials, Org. Lett. 14 (24) (2012) 6138–6141.
[23] M. Helgesen, S.A. Gevorgyan, F.C. Krebs, R.A.J. Janssen, Substituted 2,1,3-Benzothiadiazole- and thiophene-based polymers for solar cells – introducing a new thermocleavable precursor, Chem. Mater. 21 (19) (2009) 4669–4675.
[24] M. Löbert, A. Mishra, C. Uhrich, M. Pfeiffer, P. Bäuerle, Synthesis and characterization of benzo- and naphtho[2,1-b:3,4-b′]dithiophene-containing oligomers for photovoltaic applications, J. Mater. Chem. C 2 (24) (2014) 4879–4892.
[25] M. Nojima, K. Kosaka, M. Kato, Y. Ohta, T. Yokozawa, Alternating intramolecular and intermolecular catalyst-transfer Suzuki-Miyaura condensation polymerization: synthesis of boronate-terminated pi-conjugated polymers using excess dibromo monomers, Macromol. Rapid Commun. 37 (1) (2015) 79–85.
[26] Y. Li, C.-Y. Chang, Y. Chen, Y. Song, C.-Z. Li, H.-L. Yip, A.K.Y. Jen, C. Li, The effect of thieno[3,2-b]thiophene on the absorption, charge mobility and photovoltaic performance of diketopyrrolopyrrole-based low bandgap conjugated polymers, J. Mater. Chem. C 1 (45) (2013) 7526–7533.
[27] G. Zhang, Y. Fu, Z. Xie, Q. Zhang, Synthesis and photovoltaic properties of new low bandgap isoindigo-based conjugated polymers, Macromolecules 44 (6) (2011) 1414–1420.
[28] D. Gedefaw, M. Tessarolo, W. Zhuang, R. Kroon, E. Wang, M. Bolognesi, M. Seri, M. Muccini, M.R. Andersson, Conjugated polymers based on benzodithiophene and fluorinated quinoxaline for bulk heterojunction solar cells: thiophene versus thieno[3,2-b]thiophene as π-conjugated spacers, Polym. Chem. 5 (6) (2014) 2083–2093.
[29] H.Y. Kim, M.H. Choi, Y.W. Han, D.K. Moon, J.R. Haw, Deep HOMO polymers comprising anthracene units for bulk heterojunction solar cells, J. Ind. Eng. Chem. 33 (2016) 209–220.
[30] M.E. Ozser, I. Yucekan, J.B. Bodapati, H. Icil, New naphthalene polyimide with unusual molar absorption coefficient and excited state properties: synthesis, photophysics and electrochemistry, J. Luminescence 143 (2013) 542–550.
[31] M. Queste, C. Cadiou, B. Pagoaga, L. Giraudet, N. Hoffmann, Synthesis and characterization of 1,7-disubstituted and 1,6,7,12-tetrasubstituted perylenetetracarboxy-3,4:9,10-diimide derivatives, New J. Chem. 34 (11) (2010) 2537–2545.
[32] M.-H. Choi, E.J. Ko, Y.W. Han, E.J. Lee, D.K. Moon, Control of polymer-packing orientation in thin films through chemical structure of D-A type polymers and its application in efficient photovoltaic devices, Polymer 74 (2015) 205–215.
[33] X. Guo, F.S. Kim, M.J. Seger, S.A. Jenekhe, M.D. Watson, Naphthalene diimide-based polymer semiconductors: synthesis, structure–property correlations, and n-channel and ambipolar field-effect transistors, Chem. Mater. 24 (8) (2012) 1434–1442.
[34] A. Prlj, B.F. Curchod, A. Fabrizio, L. Floryan, C. Corminboeuf, Qualitatively incorrect features in the TDDFT spectrum of thiophene-based compounds,

J. Phys. Chem. Lett. 6 (1) (2015) 13–21.
[35] X.N. Zhang, A.J. Matzger, Effect of ring fusion on the electronic absorption and emission properties of oligothiophenes, J. Org. Chem. 68 (25) (2003) 9813–9815.
[36] G. Brocks, A. Tol, Small band gap semiconducting polymers made from dye molecules: polysquaraines, J. Phys. Chem. 100 (5) (1996) 1838–1846.
[37] Y. Lee, Y.M. Nam, W.H. Jo, Enhanced device performance of polymer solar cells by planarization of quinoxaline derivative in a low-bandgap polymer, J. Mater. Chem. 21 (24) (2011) 8583–8590.
[38] H.J. Song, T.H. Lee, M.H. Han, J.Y. Lee, D.K. Moon, Synthesis of donor–acceptor polymers through control of the chemical structure: improvement of PCE by planar structure of polymer backbones, Polymer 54 (3) (2013) 1072–1079.
[39] H. Kang, K.-H. Kim, J. Choi, C. Lee, B.J. Kim, High-Performance all-polymer solar cells based on face-on stacked polymer blends with low interfacial tension, ACS Macro Lett. 3 (10) (2014) 1009–1014.
[40] J.-H. Kim, S.A. Shin, J.B. Park, C.E. Song, W.S. Shin, H. Yang, Y. Li, D.-H. Hwang, Fluorinated benzoselenadiazole-based low-band-gap polymers for high efficiency inverted single and tandem organic photovoltaic cells, Macromolecules 47 (5) (2014) 1613–1622.
[41] I. Osaka, M. Saito, T. Koganezawa, K. Takimiya, Thiophene-thiazolothiazole copolymers: significant impact of side chain composition on backbone orientation and solar cell performances, Adv. Mater. 26 (2) (2014) 331–338.
[42] S. Park, D. Seo, T.I. Ryu, G. Ahn, K. Kwak, H. Kim, C.H. Cheon, N.-G. Park, B. Kim, M.J. Ko, D.-K. Lee, J.Y. Kim, H. Kim, H.J. Son, Enhancement of organic photovoltaic efficiency via nanomorphology control using conjugated polymers incorporating fullerene compatible side-chains, Macromolecules 48 (2) (2015) 337–345.
[43] N. Blouin, A. Michaud, D. Gendron, S. Wakim, E. Blair, R. Neagu-Plesu, M. Belletete, G. Durocher, Y. Tao, M. Leclerc, Toward a rational design of poly(2,7-carbazole) derivatives for solar cells, J. Am. Chem. Soc. 130 (2) (2008) 732–742.
[44] Y.J. Cheng, S.H. Yang, C.S. Hsu, Synthesis of conjugated polymers for organic solar cell applications, Chem. Rev. 109 (11) (2009) 5868–5923.
[45] M.E. Kose, Evaluation of acceptor strength in thiophene coupled donor-acceptor chromophores for optimal design of organic photovoltaic materials, J. Phys. Chem. A 116 (51) (2012) 12503–12509.
[46] W. Lee, H. Choi, S. Hwang, J.Y. Kim, H.Y. Woo, Efficient conventional- and inverted-type photovoltaic cells using a planar alternating polythiophene copolymer, Chemistry 18 (9) (2012) 2551–2558.
[47] P.P. Boix, J. Ajuria, I. Etxebarria, R. Pacios, G. Garcia-Belmonte, J. Bisquert, Role of ZnO electron-selective layers in regular and inverted bulk heterojunction solar cells, J. Phys. Chem. Lett. 2 (5) (2011) 407–411.
[48] T.-H. Lai, S.-W. Tsang, J.R. Manders, S. Chen, F. So, Properties of interlayer for organic photovoltaics, Mater. Today 16 (11) (2013) 424–432.
[49] M. Wan, H. Zhu, J. Liu, L. Huo, Poly(benzo[2,1-b:3,4-b′]dithiophene-alt-isoindigo): a low bandgap polymer showing a high open circuit voltage in polymer solar cells, RSC Adv. 5 (1) (2015) 269–273.
[50] L. Yang, L. Yan, W. You, Organic solar cells beyond one pair of donor-acceptor: ternary blends and more, J. Phys. Chem. Lett. 4 (11) (2013) 1802–1810.
[51] M. Chan Hwang, H. Kang, K. Yu, H.-J. Yun, S.-K. Kwon, K. Lee, Y.-H. Kim, New polybenzo[1,2-b:4,5-b′]dithiophene derivative with an alkoxyphenyl side chain: applications in organic photovoltaic cells and organic semiconductors, Sol. Energy Mater. Sol. Cells 125 (2014) 39–46.
[52] T.E. Kang, H.-H. Cho, H.j. Kim, W. Lee, H. Kang, B.J. Kim, Importance of optimal composition in random terpolymer-based polymer solar cells, Macromolecules 46 (17) (2013) 6806–6813.